Adsorption dynamics of H_2 on Pd(100) from first principles

A. Lozano,*[ab] A. Gross*[c] and H.F. Busnengo*[ab]

Received 17th March 2009, Accepted 6th April 2009
First published as an Advance Article on the web
DOI: 10.1039/b905432b

We study H_2 dissociative adsorption on Pd(100) through classical molecular dynamics (MD) calculations, using density functional theory (DFT) to describe the molecule–surface interaction potential. We employ two methods to evaluate the forces acting on the atoms along the trajectories: (i) by doing a DFT calculation (and using the Hellman–Feynman theorem) every time step, and (ii) by computing the gradient of a six-dimensional potential energy surface (PES) obtained first, by interpolation of DFT total energy results using the corrugation reducing procedure (CRP). The corresponding MD calculations, hereafter referred to as *ab initio* MD (AIMD) and CRP-PES-MD, respectively, provide very similar dissociative adsoption probabilities (P_{diss}) as a function of the impact energy (E_i) for initial rotational states characterized by $0 \leq J \leq 4$ indicating that the interpolated CRP-PES gives a faithful representation of the underlying *ab initio* PES. Thus, we make use of the computationally *cheaper* CRP-PES-MD for a detailed analysis of rotational effects on dissociative adsorption for $0 \leq J \leq 12$. In agreement with available experimental data for H_2 interacting with Pd surfaces, we have found that P_{diss} barely depends on J for $E_i \geq 200$ meV, and that it follows a non-monotonic J-dependence at low energies. Our simulations show that two competing dynamical effects which were previously suggested based on lower-dimensional model calculations are indeed also operative at low energies in a realistic high-dimensional treatment. For low values of J, a shadowing effect prevails that entails a decrease of P_{diss} when J increases, whereas for $J > 6$, rotational effects are dominated by the adiabatic energy transfer from rotation to perpendicular motion that provokes the increase of P_{diss} with increasing J.

I. Introduction

The adsorption of H_2 on Pd surfaces has historically attracted a lot of attention due to the well known catalytic properties of Pd (*e.g.* for hydrogenation reactions) and its potentiality as a hydrogen storage medium (see ref. 1 and references therein). Experimentally, the adsorption dynamics of H_2 on Pd surfaces has been studied by using both supersonic molecular beam[2–6] and rotational state resolved desorption[7–9] experiments. These experiments have been mainly focused on the effect of the initial kinetic energy and rotational motion of the H_2 molecules on the adsorption probability and today, it is widely accepted that: (i) dissociative adsorption of H_2 on bare Pd surfaces is a nonactivated process;[2] (ii) the sticking probability as a function of the initial kinetic energy presents a non-monotonic dependence;[3] (iii) at low kinetic energies, initial rotation slightly suppress adsorption;[4] (iv) H_2 molecules initially rotating in *helicopter* fashion adsorb with a higher probability than in *cartwheel* states.[7]

Theoretically, high dimensional quantum[10–18] and classical[11,18–23] dynamics studies have been carried out for H_2 interacting with the three lowest Miller index Pd surfaces, *i.e.* (100), (110) and (111). The latter studies made use of the Born–Oppenheimer and the so-called rigid surface (RS) approximations, *i.e.* the effect of electron-hole pair excitations is neglected and surface atoms are considered *frozen* in their equilibrium positions during the adsorption process. Thus, the H_2-surface interaction is given by a six dimensional potential (the potential energy surface, PES) usually obtained from density functional theory (DFT) results (see ref. 24, 25 and references therein).

Due to the huge number of evaluations of the PES (and/or its derivatives) required by a dynamical calculation and the high computational cost of DFT calculations, the usual approach is to obtain first a continuous representation of the PES by interpolation or fitting of a selected set of DFT data. This allows to evaluate the potential and its derivatives for any molecular configuration much (various orders of magnitude) faster than through a direct DFT calculation which reduces tremendously the time consumed by the dynamics calculations. The price to pay is the possible inaccuracy of the dynamics description due to the unavoidable errors of any PES parametrization procedure. Various methods have been proposed to represent six-dimensional (6D) PESs,[26–30] being the corrugation reducing procedure (CRP)[27] one of the most widely employed so far.

The accuracy of various CRP-PESs has been gauged by comparison with DFT results for molecular configurations not included in the interpolation input data set.[20,31,32] Typical

[a] *Instituto de Física Rosario (CONICET-UNR), Av. Pellegrini 250, 2000, Rosario, Argentina. E-mail: lozano@ifir-conicet.gov.ar*
[b] *Facultad de Ciencias Exactas, Ingeniería y Agrimensura, Universidad Nacional de Rosario, Av. Pellegrini 250, 2000 Rosario, Argentina. E-mail: busnengo@ifir-conicet.gov.ar*
[c] *Institute of Theoretical Chemistry, University of Ulm, 89069, Ulm, Germany. E-mail: axel.gross@uni-ulm.de*

errors found for H_2 are between 20–50 meV depending on the region of configuration space (*i.e.* entrance or exit channel) considered. Such small errors are expected to have a very small effect on the dynamics. However, it has been shown that for non-activated processes in particular the dynamics are very sensitive to small changes in the PES, especially at low energies.[30] Therefore, possible artifacts introduced by the continuous representation of the PES employed, cannot be completely ruled out *a priori*.

Very recently, the so-called *ab initio* molecular dynamics (AIMD) calculations (*i.e.* with the forces needed in the dynamics being directly computed using DFT through the Hellman–Feynman theorem) have also been carried out for H_2/Pd(100) and H_2/Pd(111).[33] The most important advantage of AIMD is that it allows to go beyond the RS approximation, accounting for energy exchange with surface atoms as well as surface coverage effects in a straightforward manner.[33] Since AIMD bypass any PES parametrization, it also can be used to check the reliability of a 6D PES representation method to provide artifact-free dynamical results. This is still important because the applicability of AIMD remains limited to favorable cases in which, for instance, the probabilities of interest are large enough to obtain good statistics with a moderated number of trajectories and when the total integration time required is not too long. Moreover, a detailed analysis of high dimensional dynamical results sometimes requires a large number of additional test calculations which might become too expensive using AIMD.

For H_2/Pd(100), the adsorption probability as a function of the initial translational energy and the rotational state of impinging molecules had been previously investigated using various parametrized PESs based on DFT results.[10–13] Though the qualitative energy dependence of the adsorption probability obtained in the latter studies was later confirmed by AIMD results (for initially non-rotating molecules), significant quantitative differences do exist.[33] Thus, for instance, the conclusions of ref. 13 (based on a model PES) cannot be considered as definitive, and it is important to revisit rotational effects for H_2/Pd(100) using AIMD calculations.

In this work we study the role of initial rotation on the adsorption of H_2 molecules on Pd(100) using both, AIMD and MD based on a CRP-PES, hereafter referred to as CRP-PES-MD. In section II we briefly describe the method employed to build the CRP-PES from DFT results for H_2/Pd(100) and summarize the two methods used in the dynamics calculations. Then, in section III we compare the dissociative adsorption probabilities obtained from AIMD and CRP-PES-MD calculations for various initial kinetic energies and rotational states of the impinging molecules. In view of the very good agreement between the CRP-PES-MD and AIMD results, we employ the computationally *cheaper* CRP-PES-MD to analyze in detail the origin of the main rotational effects observed. Finally, section IV summarizes the main conclusions of our study.

II. Computational methods

Both, AIMD and CRP-PES-MD are based on DFT calculations which were carried out with the *Vienna Ab initio Simulation Program* (VASP)[34–37] that uses a plane wave basis set for the electronic orbitals. Electronic exchange and correlation has been described within the generalized gradient approximation proposed by Perdew and Wang (PW91).[38] All DFT calculations were spin restricted. This is well justified for H_2 interacting with a non-magnetic metal surface at low energies (*e.g.* lower than $\sim$1.5 eV), because throughout the energetically accessible region of configuration space (*i.e.* for 0.5 Å $\leq r \leq$ 1.2 Å and $Z_{cm} \geq$ 2 Å or for any value of r and both H atoms closer than $\sim$2 Å from the surface[11]), the electronic ground state of the H_2-surface system is a singlet state.

Since, the DFT calculations for the CRP interpolation were done independently of the AIMD ones, the settings employed in both DFT calculations are similar but not exactly the same. The particular settings employed in each calculation are provided separately in the following subsections.

A AIMD calculations

The AIMD simulations have been performed using ultrasoft pseudopotentials[39,40] to represent the ionic cores in order to make the calculations compatible to previous ones carried out within the same setup.[33] The one-electron valence states were expanded in plane waves with an energy cutoff of 200 eV. The (100) surface was modeled by a slab of five layers with a (2 × 2) surface unit cell using a Monkhorst–Pack grid of 5 × 5 × 1 **k**-points.

Sticking probabilities were determined by averaging over at least 200 trajectories which were started with random initial lateral positions and orientations of the H_2 molecule 4 Å above the surface. The H_2 molecules were initially non-vibrating, *i.e.*, the simulations correspond to *classical* (C) calculations.[20] The molecules were impinging on the Pd(100) surface at normal incidence with kinetic energies between 20 meV and 400 meV. The initial rotational energies used in the AIMD simulations correspond to rotational states with the quantum number $0 \leq J \leq 4$.

The AIMD simulations were performed using the Verlet algorithm[41,42] with a time step of 1 fs within the microcanonical ensemble, *i.e.*, the total energy was conserved during the simulations. This energy conservation was typically fulfilled to within ±5 meV. The substrate atoms were initially at rest corresponding to a surface temperature of T_s = 0 K, but the uppermost two layers of the Pd slab were allowed to move during the simulations. The calculated dissociative adsorption probabilities, P_{diss}, have a statistical error[43] of $\sqrt{P_{diss}(1-P_{diss})}/\sqrt{200} \leq 0.035$. A trajectory was considered to correspond to a dissociation event when the interatomic distance of the molecule exceeded 2.5 Å and to a scattering event when the molecule returned to the initial distance of 4 Å from the surface.

B CRP-PES-MD calculations

In order to obtain a continuous representation of the 6D PES for a diatomic molecule interacting with a surface, the CRP makes use of both molecule- and atom-surface calculations.[27] DFT calculations were carried out for a single atom or molecule within a (2 × 2) unit cell and using a 5 × 5 × 1 **k**-points grid. The Pd(100) surface has been represented by a

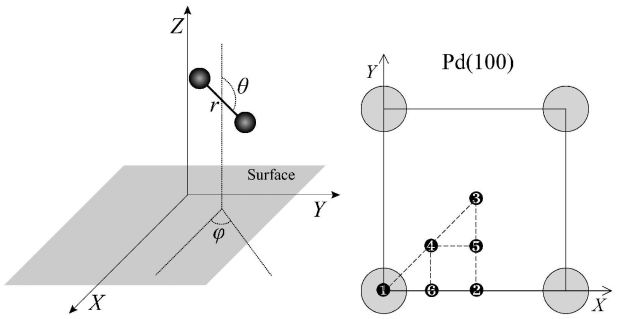

Fig. 1 Coordinates system used for H_2/Pd(100) and selected sites within the Pd(100) unit cell for which atomic and molecular DFT calculations were carried out to build the CRP-PES.

4-layer slab and a separation between consecutive slabs of ~20 Å. The interaction of electrons with the atomic cores was described within the projected augmented wave method.[44] The energy cut-off was 350 eV and electronic smearing was introduced within the Metfessel and Paxton scheme[45] with $N = 1$ and $\sigma = 0.2$ eV.

For H/Pd(100), DFT calculations have been performed on the six surface sites displayed in right panel of Fig. 1. A 3D-cubic spline has been used to interpolate the atomic interpolation function[27] from DFT results for ~30 values of Z per site, between $Z_{min} = -1.25$ Å and $Z_{max} = 5.25$ Å.

In the left panel of Fig. 1 we present the coordinate system employed throughout the text to identify different molecular configurations above the surface. We have evaluated the H_2/Pd(100) potential energy for 27 2D(Z,r) cuts with the molecular center of charge on the six high and low symmetry sites shown in Fig. 1 and various molecular orientations:

- 3 2D cuts on top (site 1: $X = 0$; $Y = 0$): ($\theta = 0°$), ($\theta = 90°$, $\varphi = 0°$) and ($\theta = 90°$, $\varphi = 45°$)
- 3 2D cuts on bridge (site 2: $X = \Delta/2$; $Y = 0$):($\theta = 0°$), ($\theta = 90°$, $\varphi = 0°$) and ($\theta = 90°$, $\varphi = 90°$)
- 3 2D cuts on hollow (site 3: $X = \Delta/2$; $Y = \Delta/2$): ($\theta = 0°$), ($\theta = 90°$, $\varphi = 0°$) and ($\theta = 90°$, $\varphi = 45°$)
- 6 2D cuts on t2h (site 4: $X = \Delta/4$; $Y = \Delta/4$): ($\theta = 0°$), ($\theta = 90°$, $\varphi = 45°$), ($\theta = 90°$, $\varphi = 135°$), ($\theta = 45°$, $\varphi = 45°$), ($\theta = 45°$, $\varphi = 135°$) and ($\theta = 45°$, $\varphi = 225°$).
- 6 2D cuts on b2h (site 5: $X = \Delta/2$; $Y = \Delta/4$): ($\theta = 0°$), ($\theta = 90°$, $\varphi = 0°$), ($\theta = 90°$, $\varphi = 90°$), ($\theta = 45°$, $\varphi = 0°$), ($\theta = 45°$, $\varphi = 90°$) and ($\theta = 45°$, $\varphi = 270°$).
- 6 2D cuts on t2b (site 6: $X = \Delta/2$; $Y = 0$): ($\theta = 0°$), ($\theta = 90°$, $\varphi = 0°$), ($\theta = 90°$, $\varphi = 90°$), ($\theta = 45°$, $\varphi = 0°$), ($\theta = 45°$, $\varphi = 90°$) and ($\theta = 45°$, $\varphi = 180°$).

where Δ is the Pd–Pd nearest neighbor distance (calculated value: 2.80 Å).

For each 2D(Z,r) cut we have computed ~210 DFT total energies (for 0.4 Å ≤ r ≤ 2.3 Å and 0.25 Å Z 4 Å). Thus, the total number of DFT (molecular and atomic) data employed is ~5850. Extrapolation of the PES toward the vacuum was carried out as explained in the appendix of ref. 20.

Using the CRP-PES, we have carried out classical MD calculations to evaluate P_{diss} for H_2 molecules impinging on Pd(100) at normal incidence for various initial kinetic energies, E_i, and rotational states (J,m_J) with $0 \leq J \leq 12$. Hamilton equations have been integrated by the predictor-corrector method of Burlisch and Stoer.[46] In the case of rotating molecules ($J \neq 0$) we have carried out calculations for a random initial orientation of the angular momentum $\mathbf{L}(|\mathbf{L}| = \sqrt{J(J+1)}$a.u.), and also for particular quantized values of L_Z ($L_Z = m_J$ a.u.). The method employed to choose the initial conditions in each case can be found elsewhere.[47] For each initial condition, (E_i,J) or (E_i,J,m_J), we have computed 5000 trajectories which makes statistical errors negligible for our proposes. We consider that dissociation has taken place whenever the H–H distance, r, reaches the value $r_{diss} = 2.25$ Å with $dr/dt > 0$. Whenever a trajectory reaches the initial value of the molecule–surface distance, $Z = 5$ Å, with velocity pointing toward the vacuum, we consider that it has been reflected. We have done both *quasi-classical* (QC) calculations, taking into account the initial vibrational zero point energy (ZPE) of H_2, and *classical* (C) calculations, without ZPE. However, we will only present C results for a consistent comparison with AIMD results and because the main conclusions that arise from the analysis of both C and QC results are essentially the same.

III. Results

A AIMD and CRP-PES-MD

In Fig. 2 we compare C dissociative adsorption probabilities obtained using AIMD,[33] P_{diss}^{AIMD}, (red triangles) and CRP-PES-MD, P_{diss}^{CRP}, (full line) for initially non-rotating molecules ($J = 0$). The agreement between P_{diss}^{AIMD} and P_{diss}^{CRP} is satisfactory. Both calculations predict the same non-monotonic energy-dependence for the sticking probability as observed experimentally. Still, a quantitative comparison with experiments is difficult because of the discrepancies between the two set of experimental data obtained by Rettner *et al.*[5] and Rendulic *et al.*[2] Due to this fact, we will mainly focus the discussion on our own theoretical results.

For initially rotating molecules with $1 \leq J \leq 4$ (Fig. 3) the agreement between P_{diss}^{AIMD} and P_{diss}^{CRP} is also very good. Both

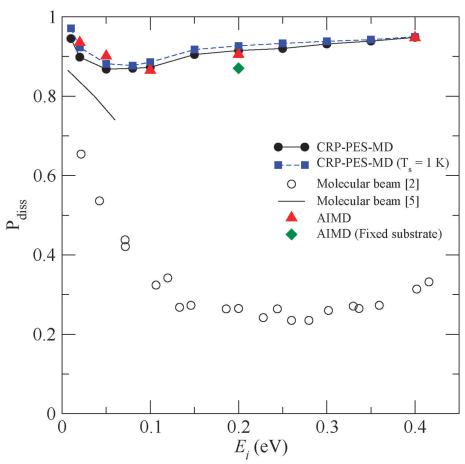

Fig. 2 Dissociative adsorption probabilities for $H_2(J = 0)$/Pd(100). Circles: P_{diss}^{CRP} for a rigid surface, squares: P_{diss}^{CRP} obtained using the surface oscillator model for a surface temperature of 1 K, triangles: P_{diss}^{AIMD},[33] diamond: P_{diss}^{AIMD} for a rigid surface[33] (see text). Experimental data: open circles,[2] black line.[5]

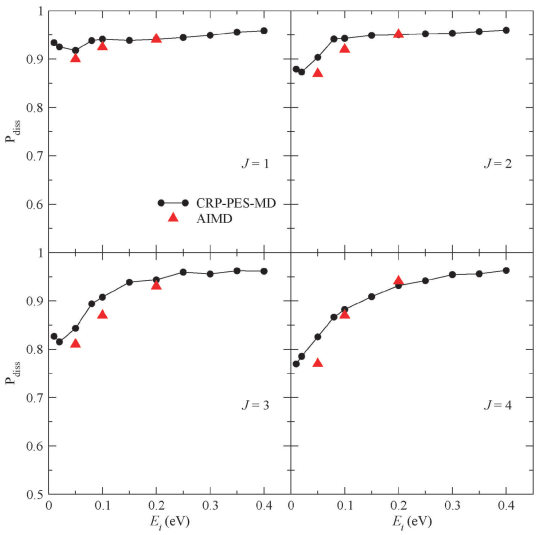

Fig. 3 $P_{diss}^{CRP}(E_i)$ (circles) and $P_{diss}^{AIMD}(E_i)$ (triangles) for $1 \leq J \leq 4$.

calculations predict the same rotational hindering effects at low translational energies and a monotonic energy-dependence of $P_{diss}(E_i)$.

It must be noted that whereas in AIMD calculations molecule–surface energy transfer has been allowed during the dynamics, the CRP-PES-MD results represented by full lines in Fig. 2 and 3 were obtained within the RS approximation. Nevertheless, in the present case, this difference should not alter dramatically the comparison. Our calculations show that H_2 dissociation on Pd(100) is essentially a direct process (see section IIIB) which in general, makes that energy transfer to the surface barely affects the dissociative adsorption probability. Additional support to this comparison, is provided by an AIMD result computed within the RS approximation for E_i = 200 meV (the diamond in Fig. 2) which is very close to the AIMD value obtained accounting for energy transfer to surface atoms for the same initial energy. Finally, we have also computed P_{diss}^{CRP} for T_s = 1 K using the surface oscillator (SO) model[48–50] (dashed line in Fig. 2) to account for energy exchange to the surface and obtained a sticking curve very close to the one obtained within the RS approximation, discrepancies being smaller than 2–3%.

We have checked that the two different setups for the underlying DFT calculations lead to equivalent results as far as the energetics are concerned. As an example, we have determined the adsorption energy of a hydrogen atom at the hollow site in a (2 × 2) geometry, *i.e.* for a hydrogen coverage of θ_H = 1/4, with respect to the free H_2 molecule. Using the setup of the AIMD calculations, we obtain an adsorption energy E_{ads} = −0.45 eV, whereas for the DFT setup underlying the CRP interpolation we obtain E_{ads} = −0.44 eV, both in good agreement with previously published values.[51] However, note that the interpolation of potential energy surfaces with a coexistence of non-activated and activated paths towards dissociative adsorption, as it is the case for the H_2/Pd(100) system, requires special attention because the dynamics in such systems is very sensitive to small changes in the PES. As was shown in a detailed study,[30] for such systems a small root mean square error between input and interpolated data does not necessarily lead imply, that reaction probabilities are faithfully reproduced on the interpolated PES. The ultimate test of the accuracy of an interpolated PES is not the root mean square error of the fitted points, but the determination of its consequences on derived properties such as calculated reaction properties. The fact that the P_{diss}^{AIMD} and P_{diss}^{CRP} agree not only as far as the dependence on the translational energy is concerned but also with respect to the initial rotational state (see Fig. 2 and 3) therefore strongly suggests that both MD simulations capture essentially the same details of the adsorption dynamics although different setups for the underlying DFT calculations were used. Therefore, in section IIIB we will employ the computationally *cheaper* CRP-PES-MD calculations to investigate in detail the origin of the rotational effects shown in Fig. 3.

B CRP-PES-MD: rotational effects

In Fig. 4 we plot the contributions of direct and indirect (dynamic trapping mediated) dissociative adsorption (P_{dir} and P_{trapp}, respectively) for J = 0, 1 and 4. We associate reactive trajectories with dynamic trapping if dissociation takes place after more than five rebounds and the others with a direct mechanism. In all cases P_{dir} is much larger than P_{trapp}. Dynamic trapping plays some role for $E_i \leq 100$ meV and P_{trapp} decreases when E_i increases. It is interesting to note that dynamic trapping for J = 0 is more important than for $J \neq 0$. For instance, at the lowest energies considered (∼10 meV) P_{trapp} = 0.3 for J = 0 and goes down to 0.1 for J = 1 and J = 4 (as well as for other values of J not shown in the Figure). For $J \neq 0$, the small contribution of dynamic trapping and the sharper increase of $P_{dir}(E_i)$ at low energies, provoke the monotonic increase of $P_{diss}(E_i)$. The particularly higher contribution of dynamic trapping for J = 0 and the relatively flat E_i-dependence of P_{dir} at low energies, give rise to the non-monotonic dependence of P_{diss} observed for J = 0 (in contrast with the case of $J \neq 0$). To summarize, Fig. 4 clearly shows that: (i) the origin of the rotational hindering effects observed for $J \neq 0$ (Fig. 3) is connected with the influence that initial rotation has on direct dissociation only, and (ii) J = 0 is a particular case in which, at low energies, dynamic trapping plays a more important role than for any value of $J \neq 0$. Accordingly, in subsections IIIB1 and IIIB2 we will consider separately the cases of $J \neq 0$ and J = 0 focussing the analysis on the direct and dynamic trapping mechanisms, respectively.

1. $J \neq 0$. In the upper panels of Fig. 5 we plot $P_{diss}(J)$ for three values of E_i: 50, 100 and 200 meV. Here we focus on P_{diss}^{CRP} (circles) but we have also included the AIMD values (triangles) for comparison. For all the three energies considered, $P_{diss}^{CRP}(J)$ presents a non-monotonic behavior, first decreasing until $J \sim 6$ and then increasing when J increases. This J-dependence is stronger at low energies (*e.g.* E_i = 50 meV) and $P_{diss}(J)$ becomes more flat when E_i increases. A similar (translational energy dependent) rotational hindering effect has been obtained in previous experimental[4] and theoretical studies[15] of dissociative adsorption of H_2 on Pd surfaces.

It is well known that in molecule–surface collisions, stereodynamical effects connected with the orientation of the angular momentum vector of impinging molecules do play an

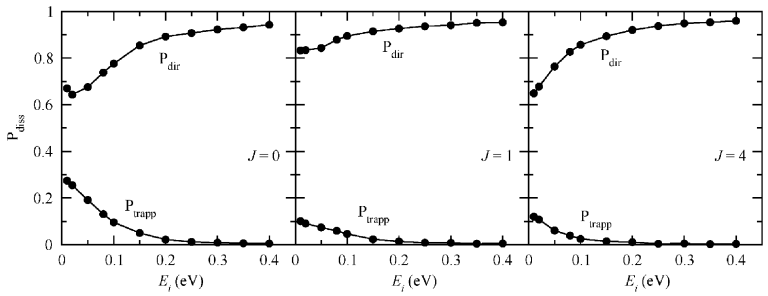

Fig. 4 Contributions of direct and trapping mechanisms to $P_{\mathrm{diss}}^{\mathrm{CRP}}(E_{\mathrm{i}})$ for $J = 0$, 1 and 4.

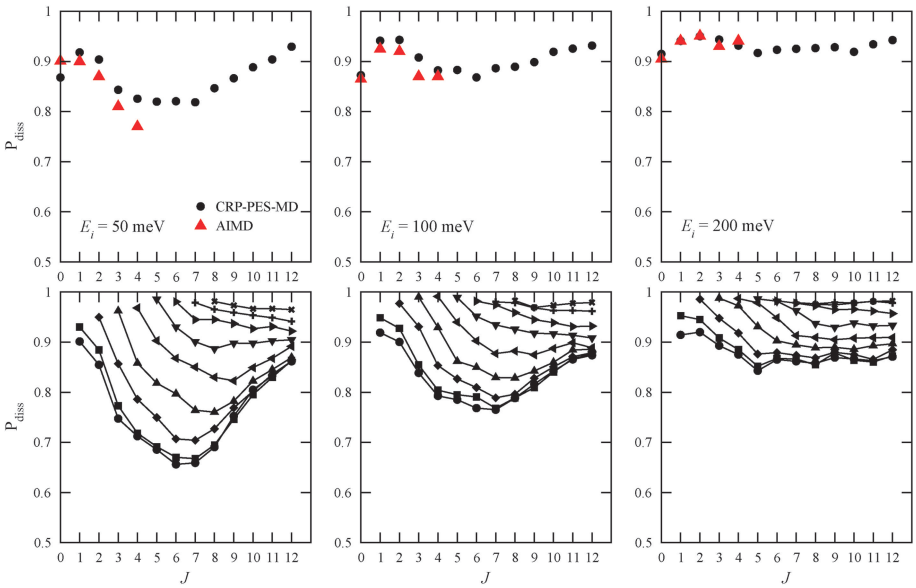

Fig. 5 Upper panels: $P_{\mathrm{diss}}(J)$ for $E_{\mathrm{i}} = 50$, 100 and 200 meV. Circles: Dynamics calculations with the CRP-PES. Triangles: AIMD calculations. Lower panels: $P_{\mathrm{diss}}(J,m_J)$ for $E_{\mathrm{i}} = 50$, 100 and 200 meV. Lines connecting an equal m_J value are included to guide the eye. Circles, $m_J = 0$; squares, $m_J = 1$; diamonds, $m_J = 2$; and so on.

important role. The dissociation probability for molecules initially rotating with the angular momentum vector approximately perpendicular and parallel to the surface (respectively referred to as helicopter and cartwheel states) are often quite different (see *e.g.* ref. 52). Thus, the behavior of $P_{\mathrm{diss}}(J)$ (averaged over m_J) can be more easily interpreted by analyzing $P_{\mathrm{diss}}(J,m_J)$ for $m_J = 0, 1, \ldots, J$. These results are presented in the lower panels of Fig. 5. To guide the eye, we have drawn lines connecting results for the same value of m_J. Thus, for example, the lowest curve corresponds to all cartwheel states ($m_J = 0$ for $J = 1, 2, \ldots, 12$). For each value of J the highest dissociation probability is always for helicopter states ($m_J = J$). On one hand, $P_{\mathrm{diss}}(J,m_J = J)$ slightly increases when J increases and reaches a saturation value close to 1. These large values are easily understood because molecules initially in helicopter states rotates in a plane parallel to the surface ($\theta = 90°$) which is particularly favorable for dissociative adsorption. On the other hand, $P_{\mathrm{diss}}(J,m_J = 0)$ presents a strong non-monotonic (first decreasing and then increasing) J-dependence that still presents $P_{\mathrm{diss}}(J)$ after averaging over m_J. This is valid in particular for $E_{\mathrm{i}} = 50$ meV but for higher energies (*e.g.* $E_{\mathrm{i}} = 200$ meV), $P_{\mathrm{diss}}(J,m_J = J)$ barely depends on J.

From the previous discussion it is clear that, in order to understand the behavior of $P_{\mathrm{diss}}(J)$, it is important to elucidate the origin of the J-dependence of $P_{\mathrm{diss}}(J,m_J = 0)$ (cartwheel states). This analysis is simplified by the fact that reflection is a direct process that takes place relatively far from the surface (between $Z \sim 1.5$ Å and 2.3 Å) and without involving significant variations of the r coordinate with respect to its initial value (*i.e.* $r = 0.75$ Å). Thus, on a given surface site the dynamics of cartwheel molecules can be approximately considered as taking place in a 2D(Z,θ)-potential. Using this model the initial decrease of $P_{\mathrm{diss}}(J,m_J = 0)$ when J increases can be interpreted in terms of a shadowing effect[53] schematically depicted in Fig. 6a. Within such a 2D(Z,θ) cut of the full dimensional PES, it is observed that when a molecule approaches the surface with a perpendicular orientation ($\theta \sim 0°$ or $\theta \sim 180°$) the PES quickly becomes repulsive, whereas for parallel configurations ($\theta \sim 90°$) a closer approach is possible (Fig. 6a).

For molecules rotating in a cartwheel state ($m_J = 0$), an increase of J entails an increase of p_θ. Thus, for a given (low) value of E_{i}, when J increases the trajectories approach a condition of grazing incidence which favors reflection into the most repulsive part of the PES for perpendicular

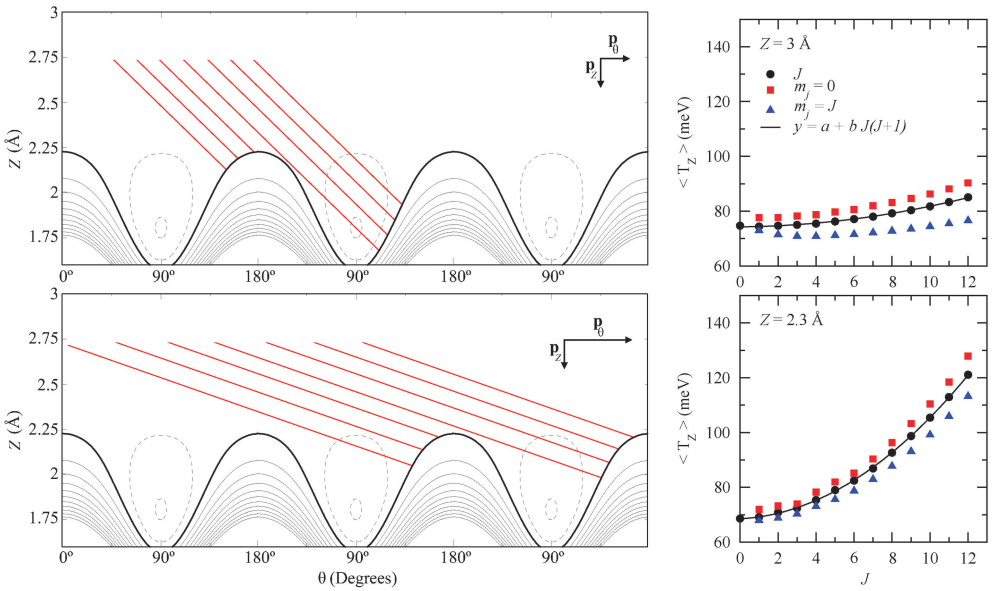

Fig. 6 (a): 2D(Z,θ) cut of the PES, distance between contour levels is 0.1 eV. Dashed contours: negative values. Full line contours: positive values. Thick contour line: 0 eV (equal to potential energy of H_2 far from the surface). Straight lines: Schematic representation of the incidence direction. Upper panel: low J values. Lower panel: large J values. (b): $\langle T_Z \rangle$ as a function of J at different values of Z for E_i = 50 meV. Circles: average over m_J, squares: m_J = 0 (cartwheel states), triangles: m_J = J (helicopter states).

configurations (lower panel of Fig. 6a). In contrast, for lower values of J the incidence condition allows a larger fraction of trajectories to approach the surface with a more convenient orientation for dissociation (upper panel of Fig. 6a). It must be kept in mind that this simplified model based on *straight line trajectories* is justified here because we are interested in direct adsorption and reflection mechanisms but would not be suitable to explain rotational effects for reflection of dynamically trapped molecules. Furthermore, it should be noted that the described mechanism is equivalent to the one invoked in order to explain the dependence of the sticking probability on the angle of incidence at energetically corrugated surfaces, *i.e.*, surfaces where the barrier height varies laterally across the surface unit cell.[54,55]

Concerning the increase of $P_{diss}(J,m_J = 0)$ for larger values of J (*e.g.* $J \geq 7$), our results show that it is due to an adiabatic energy transfer from rotation to perpendicular motion ($T_{rot} \rightarrow T_Z$) which provokes an additional acceleration of impinging molecules towards the surface favoring dissociative adsorption. Since $T_{rot} = L^2/2I = J(J+1)/2I$, with I being the moment of inertia of the molecule, when a molecule approaches the surface the interatomic bond length r and I slightly increase. In addition, our results show that in the entrance channel rotation is adiabatic (*i.e.* L^2 remains constant). Therefore, the small increase of I entails a decrease of T_{rot} (approximately proportional to $J(J+1)$) and this rotational energy lost goes to perpendicular motion. This is clearly shown by Fig. 6b where we have plotted the mean kinetic energy perpendicular to the surface as a function of J, $T_Z(J)$, when molecules reach Z = 3 Å (upper panel) and Z = 2.3 Å (lower panel). Clearly, the increase of $T_Z(J)$ when J increases is proportional to $J(J+1)$.

Therefore, for low values of J, a shadowing effect prevails producing the decrease of $P_{diss}(J,m_J = 0)$ but for larger values of J, the $T_{rot} \rightarrow T_Z$ energy transfer that favors dissociation overcompensate the effect of shadowing described in Fig. 6a and $P_{diss}(J,m_J = 0)$ increases when J increases.

It is interesting to note that the $T_{rot} \rightarrow T_Z$ energy transfer in the entrance channel is more significant for cartwheel than for helicopter states (see Fig. 6b). To understand the origin of this, we have computed the mean value of the variation of r coordinate, $\langle \Delta r \rangle$ separately for molecules rotating in cartwheel and helicopter fashion. We have found that in the former case Δr is larger than in the latter one. This explains the more efficient $T_{rot} \rightarrow T_Z$ energy transfer observed for cartwheel states. Still, why Δr is larger for molecules in a cartwheel state is, at first sight, not obvious. In fact it is so because in the entrance channel (above Z = 2.5 Å), the energetically optimum value of r for perpendicular configurations is slightly larger than for parallel configurations (see Fig. 7). Thus, molecules rotating in a cartwheel fashion in the entrance channel, visit more frequently perpendicular configurations and undergo (in average) an increase of the r coordinate slightly larger than molecules in helicopter states.

It is worth to mention that the same rotational effects are also obtained in QC calculations. Still, the difference between $P^{QC}_{diss}(J,m_J = 0)$ and $P^{QC}_{diss}(J,m_J = J)$ (cartwheel and helicopter states, respectively) is smaller than for the C results of Fig. 5 which entails a slightly weaker J-dependence of P^{QC}_{diss}.

To summarize, our analysis shows that the non-monotonic behavior of $P_{diss}(J)$ (averaged over m_J) is essentially determined by the dynamics of molecules intially rotating in cartwheel-like states, with the initial decrease due to shadowing effects and the increase above $J \sim 7$ due to the $T_{rot} \rightarrow T_Z$

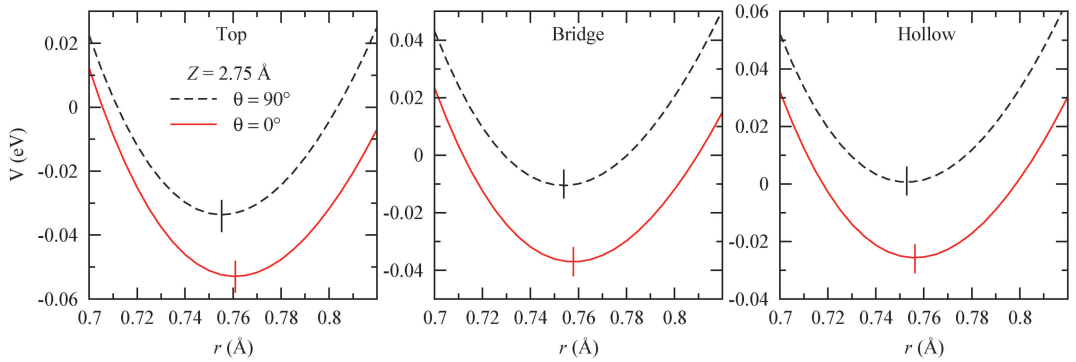

Fig. 7 Potential energy as a function of r for $Z = 2.75$ Å over the top, bridge and hollow sites. The energy minimum in each curve is indicated with a straight line. Full lines: configurations perpendicular to the surface ($\theta = 0°$), dashed lines: configurations parallel to the surface ($\theta = 90°$).

adiabatic energy transfer. This conclusions agrees very well with those obtained in previous studies for dissociation of H_2 on Pd[13,15,56] and other metal surfaces.[57]

Before concluding the analysis of rotational effects it is interesting to evaluate the quadrupole alignment parameter $A_0^{(2)}(J)$ which provides a quantitative measure of the relative sticking probability for different m_J-states for a given value of J. Moreover, $A_0^{(2)}(J)$ has been measured for H_2 molecules recombinatively desorbing from Pd(100)[7–9] and other surfaces.[52] Given that recombinative desorption corresponds to the time reversal process of dissociative adsorption, to compare with experiments, a theoretical $A_0^{(2)}(J)$ can be computed from $P_{diss}(J,m_J)$ (assuming that detailed balancing.[58] holds) through the expression,[59]

$$A_0^{(2)}(J) = \frac{\sum_{m_J=-J}^{J} \beta(J,m_J) P_{diss}(J,m_J)}{\sum_{m_J=-J}^{J} P_{diss}(J,m_J)} \qquad (1)$$

with $\beta(J,m_J) = 3m_J^2/J(J+1)-1$.

In Fig. 8 we present C results of $A_0^{(2)}(J)$ obtained for $E_i = 10$, 50 and 100 meV. $A_0^{(2)}(J)$ presents a non-monotonic behavior with a maximum value for $J \sim 6$ and going to zero for both larger and smaller values of J. A similar (less pronounced) behavior is also found in QC calculations. The fact that $A_0^{(2)} > 0$ simply put in evidence the higher values of P_{diss} for helicopter-like states compared to cartwheel-like ones. Clearly, $A_0^{(2)}$ reaches its maximum value for $J \sim 6$ because for this J value, the maximum difference between $P_{diss}(J,m_J = J)$ and $P_{diss}(J,m_J = 0)$ is obtained (see Fig. 5). The results for the alignment parameters compare well with experimental results[7] and previous high-dimensional quantum calculations.[10]

2. $J = 0$. We have found that the adsorption dynamics of initially non-rotating molecules ($J = 0$) presents some particularities not found for $J \neq 0$. For instance, in contrast with the case of $J \neq 0$, for $J = 0$ $P_{diss}(E_i)$ presents a non-monotonic behavior. This is partially because, for $J = 0$, dynamic trapping plays a more important role (twice larger at low energies) than for any other value of J. In addition, Fig. 5 shows that $P_{diss}(J = 0) < P_{diss}(J = 1)$, in contrast with the decreasing bahavior of $P_{diss}(J)$ with increasing J (for small values of J) at low energies.

To investigate the origin of this particular behavior of $P_{diss}(J = 0)$, we have computed the distribution of the polar angle θ for molecules with $J = 0$, 1 and 4 when they approach the surface in the entrance channel. These results are compared with the initial random distribution of θ at $Z = 5$ Å in Fig. 9. Our results show that for initially non rotating molecules, there is a strong change of the θ-distribution (with respect to the initial one) in favor of perpendicular configurations ($\theta \sim 0°$ or 180°). This effect is still present but more moderated already for $J = 1$ and is completely absent for $J = 4$. This strong reorientation of initially non-rotating molecules is certainly due to the fact that, in the entrance channel, the perpendicular orientation is the energetically most favorable one throughout the surface unit cell (see *e.g.* Fig. 7). Still, since the energy difference between perpendicular and parallel configurations in the entrance channel is relatively small (~20 meV at $Z = 2.75$ Å) this only affects significantly those molecules with very low initial values of p_θ and in particular,

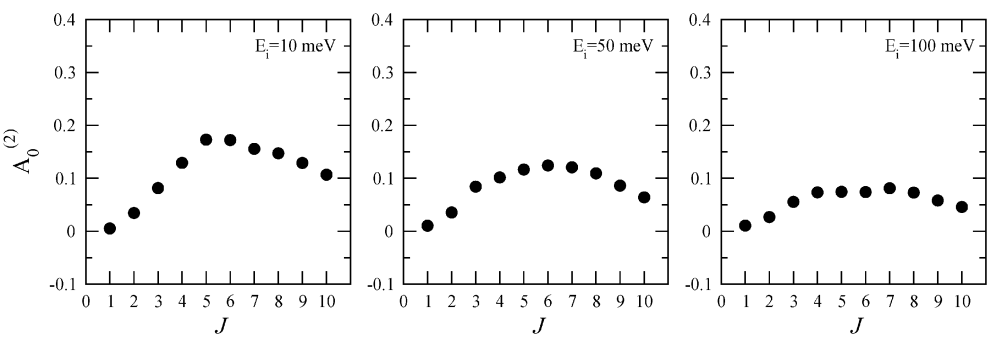

Fig. 8 $A_0^{(2)}$ as a function of J for $E_i = 10$, 50 and 100 meV.

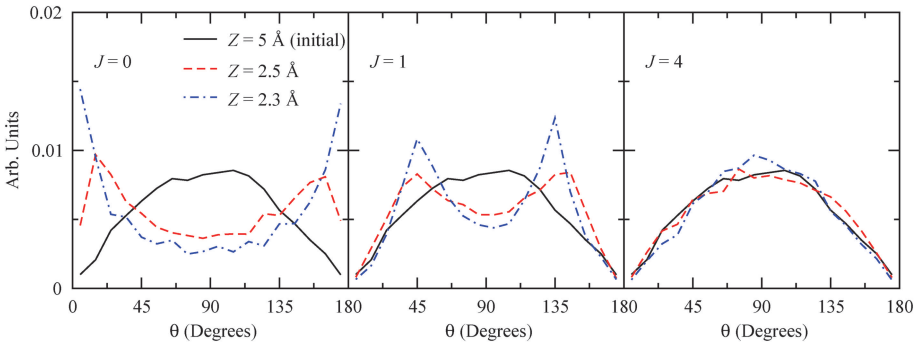

Fig. 9 θ-Distribution for molecules at different values of Z in the entrance channel for $J = 0$, 1 and 5 ($E_i = 50$ meV). Full line: $Z = 5$ Å (initial value), dashed dotted line: $Z = 3$ Å, dashed line: $Z = 2.5$ Å, dashed double dotted line: $Z = 2.3$ Å.

initially non rotating molecules. It is interesting to note that this strong reorientation of molecules in the entrance channel is also connected with relative contributions of the direct and dynamic trapping dissociation mechanisms for $J = 0$. On one hand, the reorientation of a large molecular fraction in the entrance channel towards perpendicular configurations reduces direct dissociation, because molecules cannot dissociate in such a configuration.

On the other hand, this stronger molecular reorientation for $J = 0$ in the entrance channel also entails an increase of rotational energy corresponding to a $T_Z \rightarrow T_{rot}$ transfer which provokes the increase of dynamic trapping mediated dissociation at very low energies.

This is because it is unlikely that, after acquiring some rotational energy, the molecules could later transfer all this rotational energy back to perpendicular motion as required to escape to the vacuum. Thus, in the presence of non-activated pathways to dissociation, most of these dynamically trapped molecules finally dissociate.

IV. Conclusions

We have studied H_2 dissociative adsorption on Pd(100) from classical molecular dynamics (MD) calculations using density functional theory to describe the molecule–surface interaction potential. We have first compared dissociative adsorption probabilities, P_{diss}, obtained using two different methods: (i) the so-called *ab initio* molecular dynamics (AIMD), in which the forces acting on the molecular and surface atoms are evaluated directly using DFT every time step; and (ii) MD calculations that make use of a potential energy surface (PES) obtained first by interpolation of a set of ~6000 DFT total energy results using the corrugation reducing procedure, referred to as CRP-PES-MD. For molecules impinging at normal incidence for initial rotational states from $J = 0$ up to $J = 4$ and for various impinging energies $0 \leq E_i \leq 200$ meV, both MD calculations predict the same E_i- and J-dependence of P_{diss}, indicating that the interpolated CRP-PES-MD reproduces the underlying *ab initio* PES rather well. Thus, the computationally *cheaper* MD method, *i.e.* the CRP-PES-MD was used for a detailed investigation of the adsorption dynamics. For $J = 0$, we obtain a non-monotonic E_i-dependence of P_{diss} due to an initial decreasing contribution of dynamic trapping and an increasing contribution of direct dissociation. For $J \neq 0$, dynamic trapping plays a minor role (independently of the value of J) and $P_{diss}(J)$ presents a non-monotonic dependence at low energies whereas it barely depends on J for $E_i \geq 200$ meV.

We conclude that the decrease of $P_{diss}(J)$ for low values of J (below $J \sim 6$), is mainly due to a shadowing effect that entails a higher probability of encountering repulsive parts of the PES (for perpendicular configurations relatively close to the surface) for molecules rotating in a cartwheel fashion. For larger values of J, an efficient adiabatic energy transfer from rotation to perpendicular motion accelerates the molecules towards the surface enhancing P_{diss}, as suggested based on low-dimensional simulations using a model PES. Our analysis shows that the combination of these two effects would also provoke (if detailed balancing holds) a non-monotonic J-dependence of the quadrupole alignment parameter, $A_0^{(2)}(J)$, for molecules desorbing from Pd(100) with low translational kinetic energy.

The work of A. L. and H. F. B. is supported by CONICET-Argentina (project N° PIP 5248) and ANPCyT-Argentina (project N° PICT 33595).

References

1 Y. Fukai, *The Metal Hydrogen System*, Springer-Verlag, Berlin, 1993.
2 K. D. Rendulic, G. Anger and A. Winkler, *Surf. Sci.*, 1989, **208**, 404.
3 C. Resch, H. F. Berger, K. D. Rendulic and E. Bertel, *Surf. Sci.*, 1994, **316**, L1105.
4 M. Beutl, M. Riedler and K. D. Rendulic, *Chem. Phys. Lett.*, 1995, **247**, 249.
5 C. T. Rettner and D. J. Auerbach, *Chem. Phys. Lett.*, 1996, **253**, 236.
6 M. Gostein and G. O. Sitz, *J. Chem. Phys.*, 1997, **106**, 7378.
7 D. Wetzig, R. Dopheide, M. Rutkowski, R. David and H. Zacharias, *Phys. Rev. Lett.*, 1996, **76**, 463.
8 D. Wetzig, M. Rutkowski, R. Etterich, W. David and H. Zacharias, *Surf. Sci.*, 1998, **402**, 232.
9 D. Wetzig, M. Rutkowski, H. Zacharias and A. Gross, *Phys. Rev. B: Condens. Matter Mater. Phys.*, 2001, **63**, 205412.
10 A. Gross, S. Wilke and M. Scheffler, *Phys. Rev. Lett.*, 1995, **75**, 2718.
11 A. Gross and M. Scheffler, *Phys. Rev. B: Condens. Matter Mater. Phys.*, 1998, **57**, 2493.
12 A. Eichler, J. Hafner, A. Gross and M. Scheffler, *Phys. Rev. B: Condens. Matter Mater. Phys.*, 1999, **59**, 13297.
13 A. Dianat and A. Gross, *Phys. Chem. Chem. Phys.*, 2002, **4**, 4126.
14 H. F. Busnengo, E. Pijper, M. F. Somers, G. J. Kroes, A. Salin, R. A. Olsen, D. Lemoine and W. Dong, *Chem. Phys. Lett.*, 2002, **356**, 515.

15 H. F. Busnengo, E. Pijper, G. J. Kroes and A. Salin, *J. Chem. Phys.*, 2003, **119**, 12553.
16 A. Dianat and A. Gross, *J. Chem. Phys.*, 2004, **120**, 5339.
17 D. Farías, C. Díaz, P. Rivière, H. Busnengo, P. Nieto, M. Somers, G. Kroes, A. Salin and F. Martín, *Phys. Rev. Lett.*, 2004, **93**, 246104.
18 C. Díaz, M. Sommers, G. Kroes, H. Busnengo, A. Salin and F. Martín, *Phys. Rev. B: Condens. Matter Mater. Phys.*, 2005, **72**, 035401.
19 H. F. Busnengo, W. Dong, P. Sautet and A. Salin, *Phys. Rev. Lett.*, 2001, **87**, 127601.
20 H. F. Busnengo, C. Crespos, W. Dong, J. C. Rayez and A. Salin, *J. Chem. Phys.*, 2002, **116**, 9005.
21 M. A. Di Césare, H. F. Busnengo, W. Dong and A. Salin, *J. Chem. Phys.*, 2003, **118**, 11226.
22 C. Díaz, H. F. Busnengo, F. Martín and A. Salin, *J. Chem. Phys.*, 2003, **118**, 2886.
23 C. Díaz, F. Martín, H. F. Busnengo and A. Salin, *J. Chem. Phys.*, 2004, **120**, 321.
24 A. Gross, *Surf. Sci. Rep.*, 1998, **32**, 291.
25 G. Kroes, *Prog. Surf. Sci.*, 1999, **60**, 1.
26 A. Gross, M. Scheffler, M. Mehl and D. Papaconstantopoulos, *Phys. Rev. Lett.*, 1999, **82**, 1209.
27 H. F. Busnengo, A. Salin and W. Dong, *J. Chem. Phys.*, 2000, **112**, 7641.
28 C. Crespos, M. A. Collins, E. Pijper and G. J. Kroes, *Chem. Phys. Lett.*, 2003, **376**, 566.
29 J. Ludwig, D. Vlachos, A. C. T. van Duin and W. A. Goddard III, *J. Phys. Chem. B*, 2006, **110**, 4274.
30 S. Lorenz, M. Scheffler and A. Gross, *Phys. Rev. B: Condens. Matter Mater. Phys.*, 2006, **73**, 115431.
31 P. Rivière, H. F. Busnengo and F. Martín, *J. Chem. Phys.*, 2004, **121**, 751.
32 H. F. Busnengo and A. E. Martínez, *J. Phys. Chem. C*, 2008, **112**, 5579.
33 A. Gross and A. Dianat, *Phys. Rev. Lett.*, 2007, **98**, 206107.
34 G. Kresse and J. Hafner, *Phys. Rev. B: Condens. Matter Mater. Phys.*, 1993, **47**, 558.
35 G. Kresse and J. Hafner, *Phys. Rev. B: Condens. Matter Mater. Phys.*, 1993, **48**, 13115.
36 G. Kresse and J. Furthmüller, *Comput. Mater. Sci.*, 1996, **6**, 15.
37 G. Kresse and J. Furthmüller, *Phys. Rev. B: Condens. Matter Mater. Phys.*, 1996, **54**, 11169.
38 J. P. Perdew, J. A. Chevary, S. H. Vosko, K. A. Jackson, M. R. Pederson, D. J. Singh and C. Fiolhais, *Phys. Rev. B: Condens. Matter Mater. Phys.*, 1992, **46**, 6671.
39 D. Vanderbilt, *Phys. Rev. B: Condens. Matter Mater. Phys.*, 1990, **41**, 7892.
40 G. Kresse and J. Hafner, *J. Phys.: Condens. Matter*, 1994, **6**, 8245.
41 L. Verlet, *Phys. Rev.*, 1967, **159**, 98.
42 L. Verlet, *Phys. Rev.*, 1967, **165**, 201.
43 P. M. Agrawal, A. N. A. Samadh, L. M. Raff, M. T. Hagan, S. T. Bukkapatnam and R. Komanduri, *J. Chem. Phys.*, 2005, **123**, 224711.
44 G. Kresse and D. Joubert, *Phys. Rev. B: Condens. Matter Mater. Phys.*, 1999, **59**, 1758.
45 M. Methfessel and A. T. Paxton, *Phys. Rev. B: Condens. Matter Mater. Phys.*, 1989, **40**, 3616.
46 J. Stoer and R. Burlisch, *Introduction to Numerical Analysis*, Springer, New York, 1980.
47 C. Crespos, H. F. Busnengo, W. Dong and A. Salin, *J. Chem. Phys.*, 2001, **114**, 10954.
48 J. C. Polanyi and R. J. Wolf, *J. Chem. Phys.*, 1985, **82**, 1555.
49 M. Hand and J. Harris, *J. Chem. Phys.*, 1990, **92**, 7610.
50 H. F. Busnengo, M. A. Di Césare, W. Dong and A. Salin, *Phys. Rev. B: Condens. Matter Mater. Phys.*, 2005, **72**, 125411.
51 W. Dong, V. Ledentu, P. Sautet, A. Eichler and J. Hafner, *Surf. Sci.*, 1998, **411**, 123.
52 H. Hou, S. Gulding, C. T. Rettner, A. M. Wodtke and D. J. Auerbach, *Science*, 1997, **277**, 80.
53 D. A. McCormack and G. J. Kroes, *Phys. Chem. Chem. Phys.*, 1999, **1**, 1359.
54 G. R. Darling and S. Holloway, *Surf. Sci.*, 1994, **304**, L461.
55 A. Gross, *J. Chem. Phys.*, 1995, **102**, 5045.
56 A. Diño, H. Kasai and A. Okiji, *Prog. Surf. Sci.*, 2000, **63**, 63.
57 G. R. Darling and S. Holloway, *J. Chem. Phys.*, 1994, **101**, 3268.
58 G. Comsa and R. David, *Surf. Sci. Rep.*, 1985, **5**, 145.
59 R. N. Zare, *Angular Momentum*, Wiley, New York, 1988.